Exact Solution for the Protected TEM Edge Mode in a PTD-Symmetric Parallel-Plate Waveguide

Enrica Martini, *Senior Member, IEEE*, Mário G. Silveirinha, *Fellow, IEEE*, and Stefano Maci, *Fellow, IEEE*

***Abstract*— A parity time-reversal duality symmetric structure constituted by a perfect electric conductor and perfect magnetic conductor (PMC) parallel plate waveguide is analyzed. This waveguide supports unimodal transverse electromagnetic (TEM) edge mode propagation protected against backscattering from a certain class of deformations and defects. The TEM solution is found in analytical form by using three different methods, namely, conformal mapping, mode-matching, and Fourier-transform methods. It is shown through numerical simulations that the mode propagation is robust with respect to deformations such as 90° bends and discontinuities such as transition to free space. Implementation of the PMC boundary conditions via both a bed of nails and a mushroom structure is also successfully investigated.**

***Index Terms*— Metasurface, parity-time-duality symmetry, topological modes.**

I. Introduction

TOPOLOGICAL edge modes (TPEMs) are the electromagnetic (EM) counterpart of the edge states in the integer quantum Hall effect that occurs due to topological phase transitions of matter, the discovery at the origin of the Nobel Prize awarded to Thouless, Haldane, and Kosterlitz in 2016 [1]. Topological methods, originally developed for electronic systems, have been generalized to EM systems, opening new and unexpected opportunities for innovation [2]–[4]. The novel aspect of TPEMs is that they can be unidirectional and thereby protected against backscattering; thus, they may enable a wave-guiding immune to the undesired effects of reflections due to disorder, imperfections, obstacles, or deformations of the propagation path. TPEM protection normally requires nonreciprocal elements [2]–[7]; however, recent studies have shown it can be also generated by reciprocal materials and thereby topological protected edge modes may arise in time-reversal invariant structures [8]–[13]. In this case, the edge modes are bidirectional but largely (in ideal cases totally) immune from backscattering due to chiral-type properties.

Furthermore, a few recent works have highlighted that a broad class of (nontopological) reciprocal systems may as well offer protection against backscattering [14]–[17]. In this case, the key property that guarantees that some propagating mode is immune to reflections is a duality link between the constitutive parameters of the relevant materials [14]–[17].

In particular, it was first shown in [16] that a wide family of bidirectional (not necessarily reciprocal) N-port networks invariant under the combined action of the parity (P), time-reversal (reciprocity) (T), and duality (D) operators, is characterized by a scattering matrix with $s_{11} = \cdots = s_{NN} = 0$. Thus, a parity time-reversal duality (PTD)-invariant microwave network is always matched at all ports. Thereby, PTD-invariant platforms may support waves that are insensitive to any form of perturbations or defects that do not break the PTD symmetry. This scattering anomaly (i.e., the absence of backscattering in a bidirectional system) is the optics analog of the quantum-spin-Hall effect in quantum mechanics [16]. Note that the number of ports is not necessarily identical to the number of physical waveguides because it may happen that a certain guide supports multiple modes. The condition $s_{ii} = 0$ guarantees that the energy coupled to a generic single-mode waveguide is rerouted to the other waveguides with no back reflections. When a waveguide supports two or more propagating modes, some of the energy coupled to it may return back due to modal conversion. As detailed in [16], when a waveguide supports an odd number, e.g., $1, 3, 5, \ldots$, of propagating modes it is always possible to find some suitable excitation that guarantees that no power is returned back via modal conversion [16].

Different from topological systems, the PTD invariance is not a global property but rather a single-frequency condition. Rather remarkably, PTD-systems can be formed by reciprocal materials [15], [16]. Hence, the PTD symmetry only requires reciprocal metamaterials, and this renders the fabrication quite convenient. The relative permittivity ($\bar{\bar{\varepsilon}}$) and permeability ($\bar{\bar{\mu}}$) tensors of a PTD-invariant system are linked as $\bar{\bar{\varepsilon}}(x, y, z) = \mathbf{V} \cdot \bar{\bar{\mu}}^T(x, y, -z) \cdot \mathbf{V}$, where the superscript T denotes transpose and $\mathbf{V}$ is a tensor represented by a diagonal matrix with diagonal elements $\{1, 1, -1\}$ [16]. Furthermore, the magneto-electric tensor $\bar{\bar{\xi}}$, associated with a bianisotropic response, if not zero, must satisfy the condition

Manuscript received July 18, 2018; revised September 25, 2018; accepted October 26, 2018. Date of publication November 9, 2018; date of current version February 5, 2019. This work was supported in part by European Regional Development Fund through the Competitiveness and Internationalization Operational Programme (COMPETE 2020) of the Portugal 2020 Framework, Project RETIOT, under Grant POCI-01-0145-FEDER-016432 and in part by the Fundação para Ciência e a Tecnologia under Project PTDC/EEITEL/4543/2014 and Project UID/EEA/50008/2017. *(Corresponding author: Stefano Maci.)*

E. Martini is with Wave-Up Srl, 53100 Siena, Italy (e-mail: enrica.martini@wave-up.it).

M. G. Silveirinha is with the Instituto Superior Técnico, University of Lisbon, 1649-004 Lisbon, Portugal, and also with the Instituto de Telecomunicações, 1049-001 Lisbon, Portugal (e-mail: mario.silveirinha@co.it.pt).

S. Maci is with the Department of Information Engineering and Mathematics, University of Siena, 53100 Siena, Italy (e-mail: macis@dii.unisi.it).

Color versions of one or more of the figures in this paper are available online at http://ieeexplore.ieee.org.

Digital Object Identifier 10.1109/TAP.2018.2880091

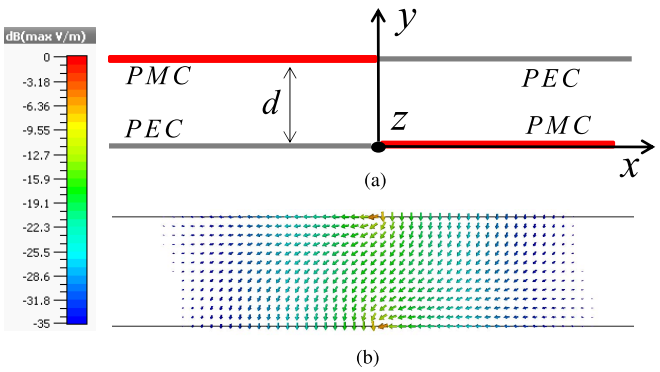

Fig. 1. (a) Geometry of the canonical problem. (b) Distribution of the transverse electric field obtained from CST Microwave Studio for the dominant TEM mode.

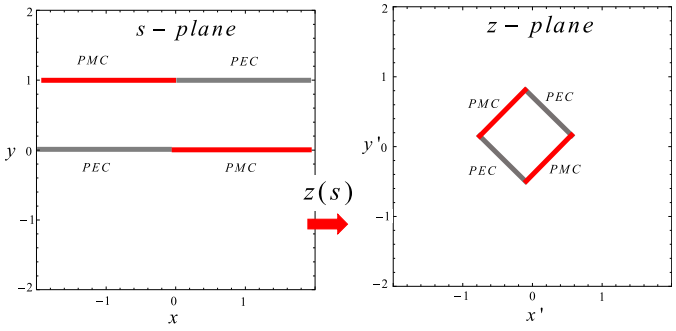

Fig. 2. Transformation of the domain by the function $z(s)$.

$\bar{\bar{\xi}}(x, y, z) = -\mathbf{V} \cdot \bar{\bar{\xi}}^T(x, y, -z) \cdot \mathbf{V}$ [16]. In the previous formulas, it is implicit that the parity transformation is $(x, y, z) \to (x, y, -z)$ but other choices are possible. Note that the topological insulators introduced by Khanikaev *et al.* [10] are particular examples of PTD-symmetric systems with an Ω-type bianisotropic coupling [16]. Furthermore, the edge waveguide described in [18] is also a PTD-invariant.

In this paper, we analyze in detail the fundamental mode of a (nonbianisotropic) PTD-symmetric guide formed by pairing two dual parallel-plate waveguides (PPWs) with a perfect electric conductor (PEC) and perfect magnetic conductor (PMC) walls. This structure was first proposed and numerically investigated in [15]. Here, we obtain an analytical exact solution for the fundamental mode. It is shown that while individual waveguides exhibit cutoff bandwidths from zero frequency to the frequency at which the distance between the walls is a quarter of the wavelength, their pairing generates a transverse EM (TEM) mode protected with respect to PTD-type defects. The resulting PTD-TEM mode is strongly confined along the discontinuity of the boundary conditions, with exponential penetration of the order of the distance between the walls.

This paper is organized as follows. In Section II, three forms of the exact solution for this protected TEM mode are derived, based on: 1) a conformal transformation; 2) mode matching; and 3) a Fourier-transform method. In Section III, examples of segmented protected propagation and radiation through an open-ended termination are presented. In Section IV, a design of the PMC walls using a bed of nails and a mushroom structure is studied by a full-wave analysis to show possible practical implementations. Conclusions are drawn in Section V.

II. Canonical Solution

The transverse cross section of the PTD-PPW is shown in Fig. 1(a). In this paper, we adopt $(x, y', z) \to (x, -y', z)$ as the relevant parity transformation so that the PTD condition reduces to $\varepsilon(x, y', z) = \mu(x, -y', z)$ for structures formed by simple nonbianisotropic reciprocal isotropic materials. Here, $y' = y - y_0$ with y_0 being the coordinate of the symmetry plane. Each waveguide wall is formed by PMC-PEC boundaries, and the center of symmetry is taken as the middle plane $y_0 = d/2$, being d is the height of the waveguide. Each individual PPW exhibits a bandgap from zero frequency to the cutoff frequency for which $d = \lambda/4$.

To figure out the EM-field structure we are going to find, Fig. 1(b) shows the distribution of electric field lines obtained by CST for the dominant TEM mode.

Let us now introduce the static electric potential $\psi(x, y)$, the gradient of which provides the electric field in the transverse plane: $\nabla_t \psi(x, y) = -\mathbf{e}_t(x, y)$ with $\nabla_t^2 \psi(x, y) = 0$. The boundary conditions impose that

$$\frac{\partial}{\partial y}\psi(x, 0) = 0 \quad \text{for } y = 0,\ x > 0 \tag{1}$$

$$\frac{\partial}{\partial y}\psi(x, d) = 0 \quad \text{for } y = d,\ x < 0 \tag{2}$$

$$\psi(x, 0) = -V_0/2 \quad \text{for } y = 0,\ x < 0 \tag{3}$$

$$\psi(x, d) = V_0/2 \quad \text{for } y = d,\ x > 0 \tag{4}$$

where V_0 is the difference of potential between the top and bottom PEC plates. The last two equations impose the potential $\pm V_0/2$ on the two PEC parts of the waveguide.

A. Conformal Mapping

The electrostatic problem can be solved by transforming the original domain into a domain in which the solution is known in a simple form. Using a combination of two Schwarz-Christoffel transformations, it is indeed possible to map the original problem in Fig. 1 (in which for simplicity, $d = 1$) into a tilted square with lateral side equal to 1 (Fig. 2).

In this domain, the potential is simply obtained by

$$\phi(z) = V_0 \mathrm{Re}\{z e^{-j\pi/4}\} \tag{5}$$

where $z = x' + jy'$ are the coordinates of the transformed domain. The relevant conformal mapping from the original domain $0 < \mathrm{Im}\{s\} < d = 1$ into the square is given by

$$z(s) = e^{j\pi/4}\left[\frac{j F_2(\xi(s))}{F_{-1}\left(\frac{\pi}{2}\right)} - (1 + j)\frac{1}{2}\right] \tag{6}$$

where $\xi(s) = \arcsin((1 - \coth(\pi s/2))^{-1/2})$ and

$$F_m(\xi) = \int_0^{\xi} d\theta \frac{1}{\sqrt{1 - m\sin^2\theta}} \tag{7}$$

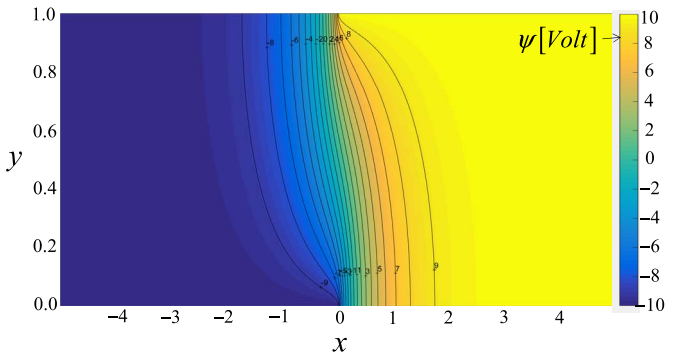

Fig. 3. Distribution of the potential $\psi(x, y)$ for $d = 1$ and $V_0 = 20$ [V] calculated through the conformal mapping solution (8).

is the incomplete elliptic integral of the first kind. Finally, one can find the solution as $\psi(x, y) = \phi(z(s/d))$ with $s = x + jy$. This leads to the following form of the potential:

$$\psi(x, y) = V_0 \mathrm{Re}\left[\frac{j}{F_{-1}\left(\frac{\pi}{2}\right)} \int_0^{\xi\left(\frac{x}{d}+j\frac{y}{d}\right)} \frac{1}{\sqrt{1-2\sin^2\theta}} d\theta\right] - \frac{V_0}{2} \tag{8}$$

$$\xi(x + jy) = \arcsin\left(\left(1 - \coth\left(\frac{\pi(x + jy)}{2}\right)\right)^{-1/2}\right). \tag{9}$$

Fig. 3 shows the equipotential contour lines for the case $d = 1$ (note that the behavior for a generic value of d is obtained by normalizing both the space coordinates by d).

B. Mode Matching

The two-part problem can be solved by mode matching at $x = 0$ after expanding the potential in both regions, $x < 0$ and $x > 0$, in terms of a complete set of functions which respect the boundary conditions and the Laplace equation.

For the sake of convenience, we construct the solution in terms of the discontinuous potential $\varphi(x, y)$ defined as

$$\varphi(x, y) = \psi(x, y) - \mathrm{sgn}(x) V_0/2 \tag{10}$$

where $\mathrm{sgn}(x)$ is the function which is 1 for positive x and -1 for negative$x$. Although the introduction of the discontinuous potential $\varphi(x, y)$ is not essential in finding the solution, it simplifies the following derivation, because $\varphi(x, y)$ satisfies conventional Dirichlet and Neumann boundary conditions. Indeed, according to (1)–(4), the function $\varphi(x, y)$ respects

$$\frac{\partial}{\partial y}\varphi(x, 0) = 0 \quad \text{for } y = 0,\ x > 0 \tag{11}$$

$$\frac{\partial}{\partial y}\varphi(x, d) = 0 \quad \text{for } y = d,\ x < 0 \tag{12}$$

$$\varphi(x, 0) = 0 \quad \text{for } y = 0,\ x < 0 \tag{13}$$

$$\varphi(x, d) = 0 \quad \text{for } y = d,\ x > 0. \tag{14}$$

Furthermore, φ goes to zero for $|x| \to \infty$. Also, $\varphi(x, y)$ respects $\nabla^2\varphi(x, y) = -\nabla^2[\mathrm{sgn}(x)V_0/2]$, i.e.,

$$\nabla_t^2\varphi(x, y) = -V_0\delta'(x) \tag{15}$$

which implies $\nabla_t^2\varphi(x, y) = 0$ for $x \neq 0$. Hence, for each of the relevant domains ($x < 0$ or $x > 0$), $\varphi(x, y)$ can be expanded into a set of functions satisfying $\nabla_t^2\varphi_n(x, y) = 0$ and the relevant boundary conditions. A complete set of functions with these properties is

$$\begin{aligned}\varphi_n^s(x, y) &= \sin(\alpha_n y)e^{-\alpha_n|x|} \quad x < 0\\ \varphi_n^c(x, y) &= -\sin(\alpha_n(d - y))e^{-\alpha_n|x|} \quad x > 0 \quad n = 0, 1, 2\ldots\end{aligned} \tag{16}$$

with $\alpha_n d = (n\pi + \pi/2)$. Note that we can also write $\varphi_n^c(x, y) = (-1)^{n+1}\cos(\alpha_n y)e^{-\alpha_n|x|}$. The function $\varphi(x, y)$ is therefore represented as

$$\varphi(x, y) = \sum_{n=0}^{\infty} a_n\varphi_n^s(x, y) \quad x < 0 \tag{17}$$

$$\varphi(x, y) = \sum_{n=0}^{\infty} b_n\varphi_n^c(x, y) \quad x > 0. \tag{18}$$

Due to the symmetry of the problem, it is necessary that $\varphi(x, y) = -\varphi(-x, d - y)$. Hence, observing that $\varphi_n^s(x, y) = -\varphi_n^c(-x, d - y)$, we find that $b_n = a_n$. Since the potential $\psi(x, y)$ in (10) is continuous, $\varphi(x, y)$ is discontinuous at $x = 0$, and its discontinuity is equal to V_0. This implies the condition

$$\sum_{n=0}^{\infty} a_n\{\sin(\alpha_n y) + \sin[\alpha_n(d - y)]\} = V_0. \tag{19}$$

Similar conditions are found by imposing the continuity of the derivative with respect to x and y

$$\sum_{n=0}^{\infty} a_n\alpha_n\{\sin(\alpha_n y) - \sin[\alpha_n(d - y)]\} = 0 \tag{20}$$

$$\sum_{n=0}^{\infty} a_n\alpha_n\{\cos(\alpha_n y) - \cos[\alpha_n(d - y)]\} = 0. \tag{21}$$

Projecting both the right- and left-hand sides of (19)–(21) onto the functions $\sin(\alpha_m y)$ yields three infinite linear systems ($i = 0, 1, 2$)

$$\sum_{n=0}^{\infty} \zeta_{mn}^{(i)} a_n = V_m^{(i)}, \quad m = 0, 1, 2\ldots \tag{22}$$

where the expressions of $\zeta_{mn}^{(i)}$ and $V_m^{(i)}$ are given in Appendix A. On the basis of the analytical form expressions of these coefficients, given in (44)–(48) of Appendix A, and after some algebraic manipulations of (22) which do not invoke other properties of the boundary value problem, one obtains

$$\sum_{n=0}^{\infty} a_{2n}\frac{4n + 1}{2n - (2m - 1)} = 0 \quad m = 1, 2, 3\ldots \tag{23}$$

$$\sum_{n=0}^{\infty} a_{2n} = V_0 \tag{24}$$

$$a_{2n+1} = 0 \quad n = 0, 1, 2\ldots \tag{25}$$

The coefficients a_n can be found in a closed form from (23)–(25) following the residue-calculus method suggested

in [19, p. 647 ff.]. According to this method, one needs to find a meromorphic function $f(z)$ of the complex variable z, with zero residue at infinity, such that (23) can be interpreted as the vanishing summation of the residues of $f(z)/[\exp(jz\pi)+1]$. The function $f(z)$ can be written as $f(z)=\sum_{n=0}^{\infty} a_{2n}((4n+1)/(z-2n))$; it has poles at $z=2n$ with residues $a_{2n}(4n+1)$ for $n=0,1,2,\ldots$, and zeros at $z=(2m-1)$ for $m=1,2,3,\ldots$ to cancel the poles of $1/(\exp(jz\pi)+1)$ and satisfy (23); furthermore, it should go to zero at infinity. In Appendix B, it is shown that $f(z)$ has the form

$$f(z)=C\frac{\Gamma\left(-\frac{z}{2}\right)}{\Gamma\left(-\frac{z}{2}+\frac{1}{2}\right)} \tag{26}$$

where $\Gamma(s)$ is the Gamma function and C is an arbitrary constant eventually determined through (24). The residues of this function are given by (see Appendix B)

$$R_n=KV_0\frac{(2n)!}{(n!)^2 4^n}\quad n=0,1,2,\ldots \tag{27}$$

where K is related to C by $KV_0=2C/\sqrt{\pi}$. The coefficients a_{2n} can be found through (22) imposing $a_{2n}(4n+1)=R_n$, i.e.,

$$a_{2n}=KV_0\frac{(2n)!}{(4n+1)(n!)^2 4^n}\quad n=0,1,2,\ldots \tag{28}$$

where the constant K can be found from (24), namely,

$$K=\left[\sum_{n=0}^{\infty}\frac{(2n)!}{(4n+1)(n!)^2 4^n}\right]^{-1}\approx 0.7965. \tag{29}$$

The above-mentioned coefficients, inserted into (17) and (18) give the electric potential in closed analytical form. With the substitution, $n\to 2n$ one gets the final solution as

$$\begin{aligned}\varphi(x,y)&=V_0\sum_{n=0}^{\infty}c_n e^{-\xi_n|x|}[\sin(\xi_n y)u(-x)-\cos(\xi_n y)u(x)]\\ \psi(x,y)&=\varphi(x,y)+\mathrm{sgn}(x)V_0/2\\ \xi_n d&\equiv\alpha_{2n}d=2\pi n+\frac{\pi}{2}\\ c_n&\equiv\frac{a_{2n}}{V_0}=0.7965\frac{(2n)!}{(4n+1)(n!)^2 4^n}\quad n=0,1,2,\ldots\end{aligned} \tag{30}$$

where $u(x)$ is Heaviside unit step function, which is equal to 1 for x positive and vanishes for x negative. Note that $\sum_{n=0}^{\infty}c_n=1$.

The distribution of the coefficients c_n is shown in Fig. 4. It can be seen that the series is strongly dominated by the first coefficient, that is by the modal function with $n=0$ (the first coefficient is 80% of the entire summation, which is unitary).

As a check of the result, the continuous potential $\psi(x,y)$ has been numerically calculated from (30) and compared with the one provided by (8). The results are shown in Fig. 5. As expected, the two representations provide the same result.

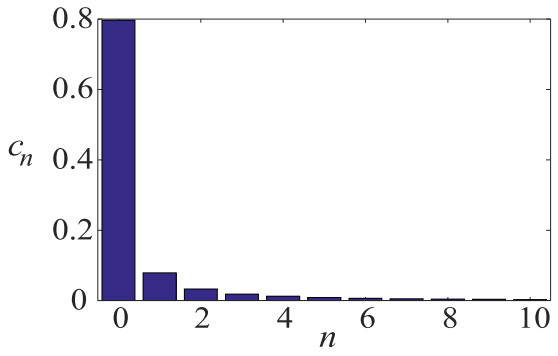

Fig. 4. Distribution of the first 10 coefficients c_n in (30).

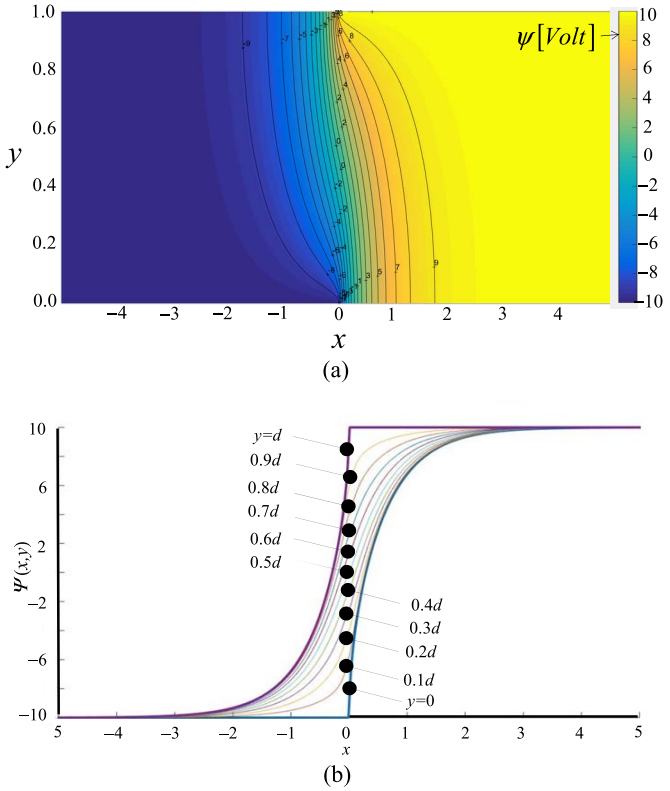

Fig. 5. (a) Distribution of the potential $\psi(x,y)$ for $d=1$ and $V_0=20$ [V] calculated through (30). This distribution is identical to the one obtained in Fig. 3 from the conformal mapping. (b) Distribution of the potential $\psi(x,y)$ as a function of x for various values of y.

C. Solution in the Fourier Domain

We can solve the problem in the Fourier-transform domain, by introducing

$$\Phi(k_x,y)=\int_{-\infty}^{\infty}\varphi(x,y)e^{jk_x x}dx. \tag{31}$$

Due to (15), $\Phi(k_x,y)$ satisfies

$$-k_x^2\Phi(k_x,y)+\frac{\partial^2\Phi}{\partial y^2}(k_x,y)=V_0 jk_x. \tag{32}$$

The function $\varphi(x,y)$ is absolutely integrable in x, and hence, $\Phi(k_x,y)$ is finite for $k_x=0$. Furthermore, $\varphi(x,y)$ is discontinuous at the origin as $\mathrm{sgn}(x)$, and hence, its Fourier transform should decay as $1/k_x$.

A suitable form for the spectrum in (31) can be derived by invoking the symmetry of the problem; this spectrum is subjected to the symmetry relation $\Phi(k_x, y) = -\Phi(-k_x, d - y)$. A solution of (32) that respects this symmetry is

$$\Phi(k_x, y) = \frac{-V_0}{jk_x}\left[A(k_x d)\frac{\sinh(k_x y)}{\sinh(k_x d)} + A(-k_x d)\frac{\sinh[k_x(d-y)]}{\sinh(k_x d)} - 1\right] \tag{33}$$

with $A(0) = 1$. It is apparent that:

1) Under condition $A(0) = 1$, the pole in $k_x = 0$ is canceled for any y, in agreement with the fact that $\varphi(x, y)$ is integrable in x.
2) Since the function $\varphi(x, y)$ is discontinuous at the origin as $\mathrm{sgn}(x)V_0/2$, $\Phi(k_x, y)$ for $k_x \to \infty$ tends to $V_0/(jk_x)$, namely, $\lim_{k_x\to\infty} jk_x\Phi(k_x, y) = V_0$ for any y. This implies that the sum of the first two terms inside the square brackets, and therefore $A(k_x d)$, should approach zero for $k_x \to \infty$.
3) The spectrum $\Psi(k_x, y)$ of the continuous function $\psi(x, y)$ can be obtained just neglecting the last unity term inside the square brackets in (33).

In order to find $A(s)$, we assume that $\varphi(x, y)$ has an expansion as in the first equation in (30), without any a priory assumption on the expression of the coefficients c_n. When this expansion is specialized for $y = 0$ and $y = d$ in (31), one obtains

$$\Phi(k_x, 0) = -V_0\sum_{n=0}^{\infty} c_n \int_0^{\infty} e^{-\xi_n x} e^{jk_x x} dx = \sum_{n=0}^{\infty}\frac{V_0 c_n}{-\xi_n + jk_x}$$
$$\Phi(k_x, d) = V_0\sum_{n=0}^{\infty} c_n \int_{-\infty}^{0} e^{\xi_n x} e^{jk_x x} dx = \sum_{n=0}^{\infty}\frac{V_0 c_n}{\xi_n + jk_x}. \tag{34}$$

The poles of $\Phi(k_x, 0)$ are all in the lower half-plane (LHP) of the complex k_x plane, because the function should be analytic in the upper half-plane (UHP) (reversely for $\Phi(k_x, d)$). The Fourier integral for a generic y should be calculated as

$$\Phi(k_x, y) = V_0\sum_{n=0}^{\infty} c_n\left[\frac{\sin(\xi_n y)}{\xi_n + jk_x} + \frac{\cos(\xi_n y)}{-\xi_n + jk_x}\right] \tag{35}$$

which is a form that automatically respects (32), under (19) and (20). One can easily see that the function $A(\pm k_x d)$ in (33) is related to $\Phi(k_x, 0)$ and $\Phi(k_x, d)$ by the equation $-V_0 A(\pm k_x d)/(jk_x) = \Phi(k_x, d; 0) - V_0/(jk_x)$. Therefore, using (34), and observing that $\lim_{k_x\to\infty} jk_x\Phi(k_x, d) = V_0$ [see 2)] implies $\sum_{n=0}^{\infty} c_n = 1$, one finds

$$A(k_x d) = -jk_x\sum_{n=0}^{\infty}\left[\frac{c_n}{\xi_n + jk_x} - \frac{1}{jk_x}\right] = \sum_{n=0}^{\infty}\frac{c_n\xi_n}{(\xi_n + jk_x)}. \tag{36}$$

We stress that the derivation of the last term in (36) does not require a particular form of the coefficients c_n, thus rendering this third method of solution independent of the second method described in Section II-B. By comparing the last term in (36) with (23) one can argue that

$$A(s) \text{ has } \textit{zeros} \text{ at } s = z_m = j\left(2\pi m - \frac{\pi}{2}\right) \quad m = 1, 2, 3\ldots$$
$$A(s) \text{ has } \textit{simple poles} \text{ at } s = j\xi_n d = j\left(2\pi n + \frac{\pi}{2}\right) \quad n = 0, 1\ldots \tag{37}$$

From these properties, one can find $A(s)$ in terms of the following ombination of Gamma functions (see Appendix C):

$$A(s) = \sum_{n=0}^{\infty}\frac{c_n\xi_n d}{(\xi_n d + js)} = \frac{\Gamma(3/4)}{\Gamma(1/4)}\frac{\Gamma\left(j\frac{s}{2\pi} + \frac{1}{4}\right)}{\Gamma\left(j\frac{s}{2\pi} + \frac{3}{4}\right)} \tag{38}$$

where the leading normalization coefficient is found imposing that $A(0) = 1$ ($\Gamma(1/4) = 3.6256, \Gamma(3/4) = 1.2254$). The Gamma function in the numerator constructs the poles of (38), and the one at the denominator constructs the zeros. Through the general expression $\Gamma(z + a)/\Gamma(z + b) \sim z^{a-b}$, the behavior at infinity can be found to be $s^{-1/2}$, which goes to zero, as expected. Upon insertion of (35) in the inverse FT

$$\varphi(x, y) = \frac{1}{2\pi}\int_{-\infty}^{\infty}\Phi(k_x, y)e^{-jk_x x}dk_x \tag{39}$$

one can recover (30) through the application of the Jordan Lemma, just summing up the residues in the LHP for x positive and in the UHP for x negative. The substitution of (38) into (33) allows for having a closed form expression for the spectrum $\Phi(k_x, y)$.

Fig. 6 shows the behavior of the spectrum of the potential for some values of y. The curves obtained by the different methods are coincident.

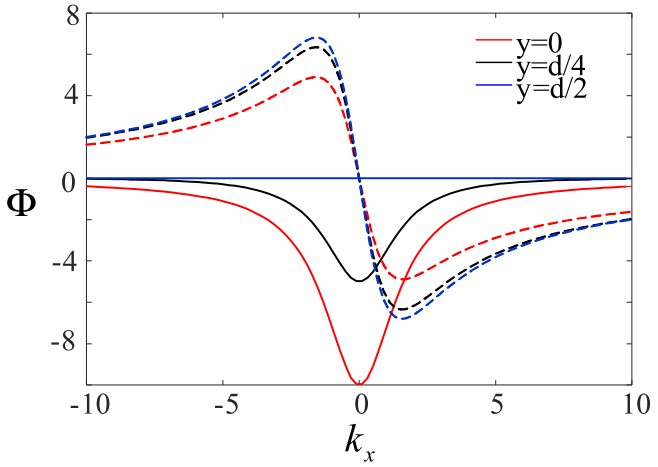

Fig. 6. Re$\{\Phi(k_x, y)\}$ (dashed line) and Im$\{\Phi(k_x, y)\}$ (solid line) for some values of y. The functions have been calculated both with (35) and with (33) using (38), leading to indistinguishable curves for any y.

III. Fields and Impedance

A. EM Fields

The fields on the transverse plane are obtained by differentiating the potential, namely, $\nabla_t\psi(x, y) = -\mathbf{e}_t(x, y)$, where $\psi(x, y) = \varphi(x, y) + \mathrm{sgn}(x)V_0/2$ and $\varphi(x, y)$ are

given by one of the alternative forms provided in Section II. Being the mode TEM, the magnetic field is given by $\mathbf{h}_t(x,y) = \hat{\mathbf{z}} \times \mathbf{e}_t(x,y)/\zeta$ where ζ is the free-space impedance. Correspondingly, the field spectra are found as $\mathbf{E}_t = (jk_x\hat{\mathbf{x}} - \hat{\mathbf{y}}\partial/\partial y)\Psi(k_x,y)$ and $\mathbf{H}_t = \hat{\mathbf{z}} \times \mathbf{E}_t/\zeta$, which can be rewritten, using (33) and (38), as

$$\begin{aligned}\mathbf{E}_t(k_x,y) &= -V_0\left[\hat{\mathbf{x}}\left(\Phi_s^+ + \Phi_s^-\right) + j\hat{\mathbf{y}}\left(\Phi_c^+ + \Phi_c^-\right)\right]\\ \mathbf{H}_t(x,y) &= -\frac{1}{\zeta}V_0\left[-j\hat{\mathbf{x}}\left(\Phi_c^+ + \Phi_c^-\right) + \hat{\mathbf{y}}\left(\Phi_s^+ + \Phi_s^-\right)\right] \quad (40)\end{aligned}$$

where

$$\begin{aligned}\Phi_s^+(k_x,k_y) &= A(k_xd)\frac{S(k_x,k_y)}{\sinh(k_xd)}\\ \Phi_c^+(k_x,k_y) &= A(k_xd)\frac{C(k_x,k_y)}{\sinh(k_xd)}\\ \Phi_s^-(k_x,k_y) &= A(-k_xd)\frac{S(k_x,-k_y)e^{jk_yd}}{\sinh(k_xd)} \quad (41)\\ \Phi_c^-(k_x,k_y) &= -A(-k_xd)\frac{C(k_x,-k_y)e^{jk_yd}}{\sinh(k_xd)}\end{aligned}$$

$$\begin{aligned}S(k_x,k_y) &= \frac{e^{jk_yd}[k_x\cosh(k_xd) - jk_y\sinh(k_xd)] - k_x}{\left(k_x^2+k_y^2\right)}\\ C(k_x,k_y) &= \frac{e^{jk_yd}[k_x\sinh(k_xd) - jk_y\cosh(k_xd)] + jk_y}{\left(k_x^2+k_y^2\right)}. \quad (42)\end{aligned}$$

The asymptotic behavior of the functions $\Psi^{\pm}(k_x,y)$ is of type $(k_xd)^{-1/2}$, which implies that the field is singular at the junctions between the PEC and PMC boundary conditions with a singularity of type $x^{-1/2}$.

B. Characteristic Impedance of the Waveguide

Being the mode TEM, the wave impedance is coincident with the free-space impedance $\zeta = 377\ \Omega$. Interestingly, the characteristic impedance $R = V_0/I_0$ of the waveguide is also equal to ζ. To show this, we calculate the current I_0 by integrating the magnetic field on the PEC portion of the waveguide. The electric current density on $y = 0$ is given by

$$\begin{aligned}I_0 &= \int_{-\infty}^{0^-}\mathbf{j}(x)\cdot\mathbf{z}dx = -\frac{1}{\zeta}\int_{-\infty}^{0^-}\frac{\partial}{\partial x}\psi(x,0)dx\\ &= -\frac{V_0}{\zeta}\sum_{n=0}^{\infty}\xi_n c_n\int_{-\infty}^{0^-}e^{-\xi_n|x|}dx = \frac{V_0}{\zeta}\sum_{n=0}^{\infty}c_n = \frac{V_0}{\zeta} \quad (43)\end{aligned}$$

where the last equality is due to the property $\sum_{n=0}^{\infty}c_n = 1$. Hence, for this structure, the characteristic impedance of the waveguide is equal to the wave impedance and to the free-space impedance. This implies a power flow equal to $P = |V_0|^2/(2\zeta)$. Note that the characteristic impedance is independent of the distance d between the plates. This can be understood with a simple dimensional analysis, noticing that there is no other characteristic length scale in the problem, and thus the characteristic impedance must be totally independent of d.

IV. Protected Propagation

Examples of protected propagation are shown in the following, with results obtained with CST Microwave Studio.

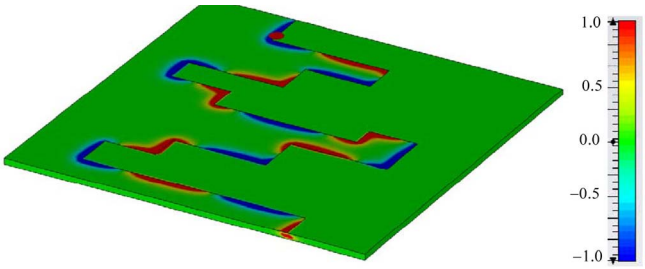

Fig. 7. Time snapshot of the y-component of the electric field excited by a point source in a segmented PTD-PPW waveguide. The represented area has electrical dimensions $2\lambda \times 2\lambda$.

A. Segmented PTD-Waveguide

In this section, we study the propagation in a segmented PTD-waveguide with ideal PEC-PMC walls (Fig. 7). The distance d between the two parallel walls has been setup as $d = 1$ cm, and the material in between the plates is air. This case serves to estimate the effect of repetitive 90° bend discontinuities on the propagation. It is seen that the propagation is protected through the entire path with the reflection coefficient precisely zero at the input port over the entire bandwidth (in the CST simulation the reflection coefficient is on the order of −25 dB due to numerical noise). Indeed, the segmented guide is PTD symmetric and for $\lambda > 4d$ the input and output ports support a single propagating mode (the TEM mode characterized in the previous sections). Hence, the system may be regarded as a two-port network and the property $s_{11} = s_{22} = 0$ guarantees that back-reflections are forbidden [16]. A snapshot of the vertical (y-component) of the electric field in the middle plane of the waveguide is presented in Fig. 7. The field is excited by a short vertical dipole radiating at 1 GHz at the junction discontinuity of boundary conditions. The colored map in Fig. 7 shows a strong confinement of the field along the line discontinuity with no diffraction losses.

B. Open Ended PEC-PMC Waveguide

The effect of opening the PTD-PPW waveguide into free space is investigated in Fig. 8. Being the free space a PTD-symmetric medium, we expect zero backreflections at the input port (note that the input port supports a single propagating mode and the PTD invariance guarantees that $s_{11} = 0$).

Fig. 8(a) shows the effect of a single PTD-PPW opened in free space. The distance between the walls is $d = 2$ mm. A time snapshot of the magnitude of the electric field at 30 GHz is visualized at the intermediate section between the two walls. The reflection coefficient has been found to be less than −20 dB all over the unimodal bandwidth. A second numerical example is obtained by pairing two close waveguides alternating PEC-PMC-PEC boundary conditions on one wall and PMC-PEC-PMC on the other wall. The distance between the two adjacent PMC-PEC junctions is 5 mm. Fig. 8(b) shows the distribution of the field magnitude when the two waveguides are excited by two modes in phase. Again, the PTD symmetry guarantees that the individual guides are matched; however, they are not necessarily isolated,

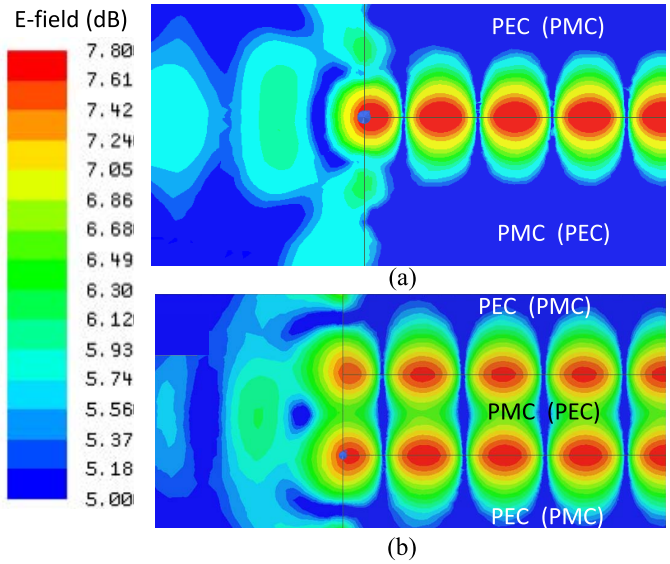

Fig. 8. PTD-PPW waveguide open in free space. (a) Single PTD-PPW (b) Double PTD-PPW fed by two TEM modes in phase. Black horizontal lines: positions of the junctions between the PEC and PMC boundaries. Black vertical lines: interface with the free space. The results are obtained using CST Microwave Studio.

hence, now it is not guaranteed that all the incoming energy is radiated toward the free-space region. The numerically calculated active reflection coefficient (which includes the effect of numerical noise) is, however, below −16 dB in this second setup, which indicates good port isolation. It is worth noticing the good matching level that is obtained despite the small value of d in terms of the wavelength.

V. Examples of Practical Implementation

A practical implementation of the PEC-PMC waveguide can be obtained by realizing equivalent high-impedance boundary conditions through a bed of nails [20], [21]. A structure formed by a bed of nails top covered by a PEC wall [see inset "A" of Fig. 9(a)] exhibits an electromagnetic bandgap (EBG) [22]–[24]. Coupling this structure with an identical one with opposite position of the pins generates a mode inside the bandgap. In the example of Fig. 9, the length of the nails is 6 times the distance d between the equivalent walls. The dispersion diagram is shown in Fig. 9(a) (calculated with CST Microwave Studio, case relevant to $d = 0.5$ mm). This diagram was obtained by solving the eigenvalue problem for a section of the structure with lateral PEC boundary conditions at a sufficiently large distance D from $x = 0$. In the simulation, we chose D such that the dominant mode [$n = 0$ in (30)] is attenuated by a factor 10 000 (this leads to $D = 5.86d$). With the selected value of $d = 0.5$ mm, the bandgap of each half of the waveguide occurs in the spectral range of 25–40 GHz [gray region in Fig. 9(a)]. The two boundaries of the bandgap correspond to $6d = [0.25–0.4]\lambda$ or equivalently $d = [0.04–0.0667]\lambda$.

In the bandgap of the top covered bed of nails [inset "A" of Fig. 9(a)], a quasi-TEM mode is found for the composite structure emulating the PTD waveguide

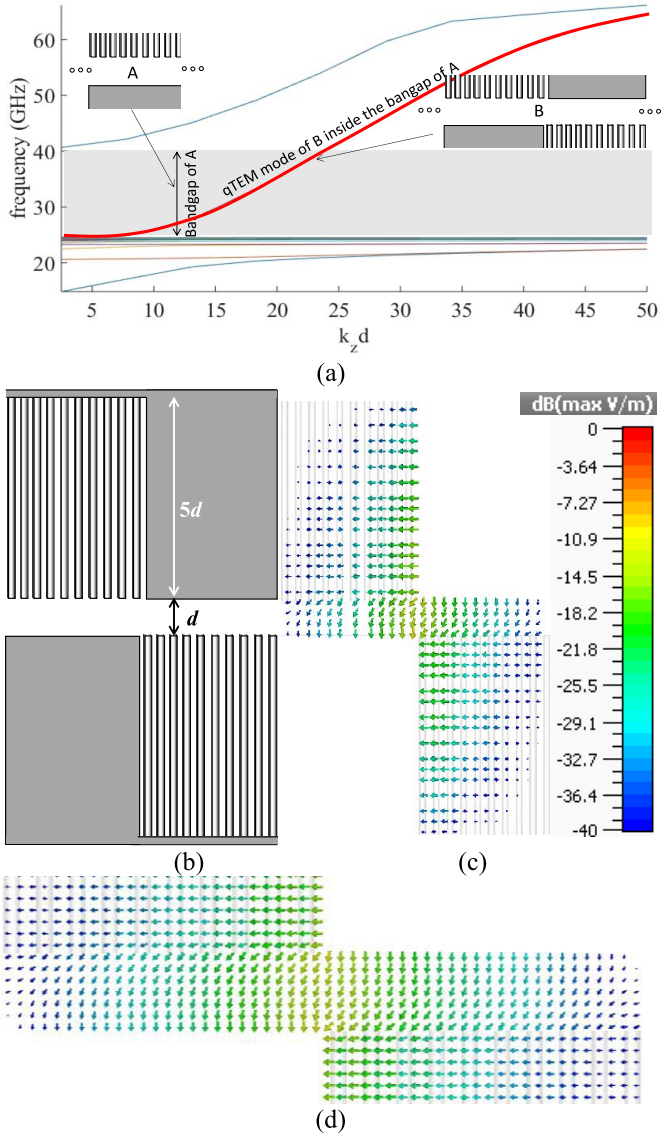

Fig. 9. (a) Dispersion diagram of modes in the PTD-waveguide with the PMC walls implemented using a bed of nails. (b) Cross section of the PTD waveguide. (c) Distribution of the electric field associated with the quasi-TEM mode. (d) Zoomed-in view of the central part.

[inset "B" of Fig. 9(a)]. This mode is quite nondispersive in the region 30–40 GHz. The dispersion curves below 25 GHz are associated with spurious modes that travel inside the multiconnected wire domain constituted by the nails region. They are present for both structures A and B in the simulation. The transverse field associated with the dominant quasi-TEM mode [Fig. 9(c) and zoomed-in view Fig. 9(d)] closely resembles the one associated with the ideal PTD waveguide [see Fig. 1(b)].

A more compact structure may be obtained by using the mushroom ground plane [25]. An example is illustrated in Fig. 10. The mushroom structure [see Fig. 10(a)] is realized with a dielectric slab of thickness 0.5 mm and relative permittivity equal to 6, and the distance between the equivalent walls is 0.5 mm. Fig. 10(b) shows the dispersion diagram of the first 14 modes supported by the structure, calculated with CST Microwave Studio. As it can be seen, there is a unimodal

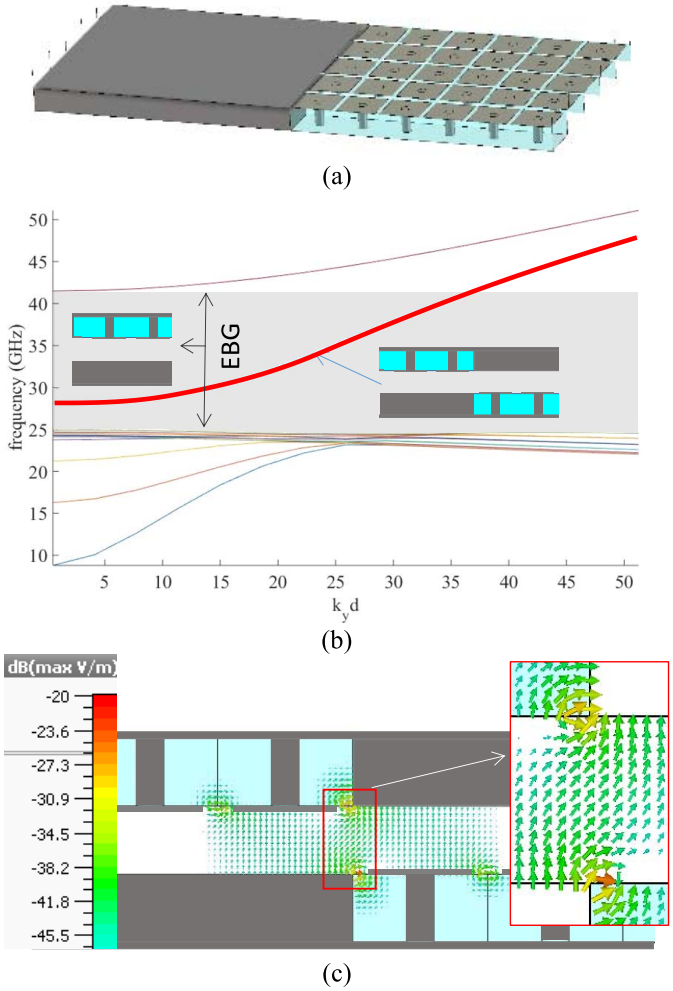

Fig. 10. PTD-waveguide with the PMC walls implemented using a mushroom ground plane. (a) Geometry of the lower half of the structure. (b) Dispersion diagram. (c) Distribution of the electric field associated with the quasi-TEM mode.

region between 28.2 and 41.4 GHz, which falls in the EBG of each half of the waveguide. The mode supported in this region is quasi-TEM, and its electric field distribution at 35 GHz is shown in Fig. 10(c). Also, in this case, the field distribution is somewhat similar to the one in the ideal PTD waveguide [see the inset of Fig. 10(c)].

VI. Conclusion

The exact solution of a PTD symmetric structure constituted by a PEC-PMC PPW has been found. This waveguide supports unimodal TEM edge mode propagation protected against backscattering deformations and defects that maintain a PTD symmetry. The exact TEM solution is found in analytical form by using three different methods, namely, by conformal mapping, by mode-matching, and by the Fourier-transform method. It is found that the three solutions are coincident and each of them highlights different aspects of the structure of the modal fields. The characteristic impedance of the TEM mode coincides with the wave impedance of the mode and with the free-space. It is also shown through numerical simulations that the mode propagation is robust with respect to deformations such as 90° bends and transition to free space, confirming that PTD symmetric reciprocal structures are matched at all ports. Implementation of the PMC boundaries via both a bed of nails and a mushroom structure is also proposed, showing a quite linear dispersion characteristic.

Appendix

A. Derivation of the Linear System for the Coefficients a_n

The linear systems $\sum_{n=0}^{\infty}\zeta_{mn}^{(i)}a_n = V_m^{(i)}$ $m = 0, 1, 2\ldots$, for $i = 0, 1, 2, \ldots$ in (22) are obtained by imposing the continuity of the potential ψ and of its derivatives at $x = 0$ through testing with the functions $\sin(\alpha_m y)$.

The coefficients of the linear systems are calculated as

$$\mathrm{V}_m^{(0)} = \mathrm{V}_0\int_0^d \sin(\alpha_m y)dy = \mathrm{V}_0\frac{d}{(m\pi+\pi/2)} \tag{44}$$

$$\mathrm{V}_m^{(i)} = 0, \quad i = 1, 2 \tag{45}$$

$$\begin{aligned}\zeta_{mn}^{(0)} &= \int_0^d [\sin(\alpha_n y) + (-1)^n\cos(\alpha_n y)]\sin(\alpha_m y)dy \\ &= \frac{d}{2}\delta_{nm} + \frac{d}{2}\left[\frac{(-1)^m(2n+1)-(-1)^n(2m+1)}{\pi(n+1+m)(n-m)}\right]\end{aligned} \tag{46}$$

$$\begin{aligned}\zeta_{mn}^{(1)} &= \int_0^d \alpha_n\left[\cos(\alpha_n y) - (-1)^n\sin(\alpha_n y)\right]\sin(\alpha_m y)dy \\ &= -\frac{d}{2}\alpha_m\delta_{nm} + \frac{d}{2}\alpha_n\left[\frac{(-1)^m(2n+1)-(-1)^n(2m+1)}{\pi(n+1+m)(n-m)}\right]\end{aligned} \tag{47}$$

$$\begin{aligned}\zeta_{mn}^{(2)} &= \int_0^d \alpha_n\left[\sin(\alpha_n y) - (-1)^n\cos(\alpha_n y)\right]\sin(\alpha_m y)dy \\ &= \alpha_m\frac{d}{2}\delta_{nm} - \frac{d}{2}\alpha_n\left[\frac{(-1)^n(2m+1)-(-1)^m(2n+1)}{\pi(n+1+m)(m-n)}\right].\end{aligned} \tag{48}$$

B. Determination of the Function $f(z)$

The function $f(z)$ in (26) should have the form

$$f(z) = p(z)\frac{\prod_{m=1}^{\infty}\left(1-\frac{z}{2m-1}\right)e^{z/2m}}{z\prod_{n=1}^{\infty}\left(1-\frac{z}{2n}\right)e^{z/2n}} \tag{49}$$

where the exponential terms have been introduced in order to ensure convergence of the infinite product. Comparing it with the definition of the gamma function, one can find that ([27], p. 59)

$$\begin{aligned}\prod_{n=1}^{\infty}\left(1-\frac{z}{2n}\right)e^{z/2n} &= -\frac{2e^{\gamma z/2}}{\Gamma\left(-\frac{z}{2}\right)z} \\ \prod_{m=1}^{\infty}\left(1-\frac{z}{2m-1}\right)e^{z/2m} &= \frac{e^{\gamma z/2}\sqrt{\pi}}{\Gamma\left(-\frac{z}{2}+\frac{1}{2}\right)}\end{aligned} \tag{50}$$

from which one has $p(z) = const.$, therefore, obtaining (26). In order to find the residues, one can use the mathematical identities

$$\begin{aligned}\Gamma\left(-\frac{z}{2}\right)\Gamma\left(\frac{z}{2}\right) &= -\frac{2\pi}{z\sin\left(\frac{z\pi}{2}\right)} \\ \Gamma\left(-\frac{z}{2}+\frac{1}{2}\right)\Gamma\left(\frac{z}{2}+\frac{1}{2}\right) &= \frac{\pi}{\cos\left(\frac{z\pi}{2}\right)}\end{aligned} \tag{51}$$

from which

$$f(z) = C\frac{\Gamma\left(-\frac{z}{2}\right)}{\Gamma\left(-\frac{z}{2}+\frac{1}{2}\right)} = -C\frac{\Gamma\left(\frac{z}{2}+\frac{1}{2}\right)}{z\Gamma\left(\frac{z}{2}\right)}2\cot\left(\frac{z\pi}{2}\right). \quad (52)$$

Note that (52) can be also rewritten by using the identity

$$\Gamma\left(\frac{z}{2}+\frac{1}{2}\right)\Gamma\left(\frac{z}{2}\right) = 2\sqrt{\pi}e^{-z\ln 2}\Gamma(z) \quad (53)$$

as

$$f(z) = -C\frac{2\sqrt{\pi}e^{-z\ln 2}\Gamma(z)}{z\left(\Gamma\left(\frac{z}{2}\right)\right)^2}2\cot\left(\frac{z\pi}{2}\right) \quad (54)$$

which is the function introduced by Collin for solving a boundary value problem of a step discontinuity [19]. The residue of the function $f(z)$ at the poles $z = 2n$ can be found as

$$\lim_{z\to 2n} f(z)(z-2n) = R_n = K'\frac{\Gamma(n+1/2)}{n\Gamma(n)} \quad n = 1, 2, \ldots$$
$$\lim_{z\to 0} f(z)z = R_0 = K'\sqrt{\pi} \quad n = 0 \quad (55)$$

where we have used $\lim_{z\to 0}[z\Gamma(z)] = 1$, $\Gamma(1/2) = \sqrt{\pi}$, and $K' = 2C/\pi$. From here, one can find the coefficients a_{2n}. Observing that $\Gamma(n) = (n-1)!$ and, from (44), that $\Gamma(n+1/2) = \sqrt{\pi}(2n)!/(4^n n!)$ one has

$$R_n = K\frac{\sqrt{\pi}(2n)!}{(n!)^2 4^n} \quad n = 1, 2, 3, \ldots \quad (56)$$

C. Construction of the Function A(s)

To construct the function $A(s)$, we use the relation $A(s) = N(s)/D(s)$ with

$$N(s) = \prod_{m=1}^{\infty}\left(1 - \frac{s}{j(2\pi m - \pi/2)}\right)e^{s/(j2\pi m)}$$
$$= \frac{2e^{\gamma s/(j2\pi)}\Gamma\left(\frac{3}{4}\right)}{\Gamma\left(\frac{js}{2\pi}+\frac{3}{4}\right)}$$
$$D(s) = \prod_{n=1}^{\infty}\left(1 - \frac{s}{j(2\pi n - 3\pi/2)}\right)e^{s/(j2\pi n)}$$
$$= \frac{2e^{\gamma s/(j2\pi)}\Gamma\left(\frac{1}{4}\right)}{\Gamma\left(\frac{js}{2\pi}+\frac{1}{4}\right)} \quad (57)$$

which can be found as the general form of the expression reported in [26] and leads to (38).

ACKNOWLEDGMENT

The authors would like to thank the collaboration of I. Rybalko for obtaining the data of Fig. 7.

REFERENCES

[1] F. D. M. Haldane, "Nobel lecture: Topological quantum matter," *Rev. Mod. Phys.*, vol. 89, no. 4, p. 040502, 2017.
[2] F. D. M. Haldane and S. Raghu, "Possible realization of directional optical waveguides in photonic crystals with broken time-reversal symmetry," *Phys. Rev. Lett.*, vol. 100, no. 1, p. 013904, 2008.
[3] S. Raghu and F. D. M. Haldane, "Analogs of quantum-Hall-effect edge states in photonic crystals," *Phys. Rev. A, Gen. Phys.*, vol. 78, no. 3, p. 033834 2008.
[4] Z. Wang, Y. Chong, J. D. Joannopoulos, and M. Soljačić, "Observation of unidirectional backscattering-immune topological electromagnetic states," *Nature*, vol. 461, pp. 772–775, Oct. 2009.
[5] H. Lira, Z. Yu, S. Fan, and M. Lipson, "Electrically driven nonreciprocity induced by interband photonic transition on a silicon chip," *Phys. Rev. Lett.*, vol. 109, no. 3, p. 033901, 2012.
[6] K. Fang and S. Fan, "Controlling the flow of light using the inhomogeneous effective gauge field that emerges from dynamic modulation," *Phys. Rev. Lett.*, vol. 111, no. 20, p. 203901, 2013.
[7] M. G. Silveirinha, "Chern invariants for continuous media," *Phys. Rev. B, Condens. Matter*, vol. 92, no. 12, p. 125153, 2015.
[8] M. C. Rechtsman *et al.*, "Photonic Floquet topological insulators," *Nature*, vol. 496, pp. 196–200, Apr. 2013.
[9] W. Gao *et al.*, "Topological photonic phase in chiral hyperbolic metamaterials," *Phys. Rev. Lett.*, vol. 114, no. 3, p. 037402, 2015.
[10] A. B. Khanikaev, S. H. Mousavi, W.-K. Tse, M. Kargarian, A. H. MacDonald, and G. Shvets, "Photonic topological insulators," *Nature Mater.*, vol. 12, no. 3, pp. 233–239, 2013.
[11] X. Cheng, C. Jouvaud, X. Ni, S. H. Mousavi, A. Z. Genack, and A. B. Khanikaev, "Robust reconfigurable electromagnetic pathways within a photonic topological insulator," *Nature Mater.*, vol. 15, no. 5, pp. 542–548, 2016.
[12] A. Slobozhanyuk, S. H. Mousavi, X. Ni, D. Smirnova, Y. S. Kivshar, and A. B. Khanikaev, "Three-dimensional all-dielectric photonic topological insulator," *Nature Photon.*, vol. 11, pp. 130–136, Dec. 2017.
[13] M. G. Silveirinha, "$\mathbb{Z}_2$ topological index for continuous photonic materials," *Phys. Rev. B, Condens. Matter*, vol. 93, no. 7, p. 075110, 2016.
[14] F. Liu and J. Li, "Gauge field optics with anisotropic media," *Phys. Rev. Lett.*, vol. 114, no. 10, p. 103902, 2015.
[15] W.-J. Chen, Z.-Q. Zhang, J.-W. Dong, and C. T. Chan, "Symmetry-protected transport in a pseudospin-polarized waveguide," *Nature Commun.*, vol. 6, Sep. 2015, Art. no. 8183.
[16] M. G. Silveirinha, "P·T·D symmetry-protected scattering anomaly in optics," *Phys. Rev. B, Condens. Matter*, vol. 95, no. 3, p. 035153, 2017.
[17] T. Van Mechelen and Z. Jacob. (2018). "Dirac-Maxwell correspondence: Spin-1 bosonic topological insulator for light." [Online]. Available: https://arxiv.org/abs/1708.08192
[18] D. J. Bisharat and D. F. Sievenpiper, "Guiding waves along an infinitesimal line between impedance surfaces," *Phys. Rev. Lett.*, vol. 119, no. 10, p. 106802, 2017.
[19] R. E. Collin, *Field Theory of Guided Waves*, 2nd ed. New York, NY, USA: IEEE Press, 1991.
[20] R. J. King, D. V. Thiel, and K. S. Park, "The synthesis of surface reactance using an artificial dielectric," *IEEE Trans. Antennas Propag.*, vol. AP-31, no. 3, pp. 471–476, May 1983.
[21] M. G. Silveirinha, C. A. Fernandes, and J. R. Costa, "Electromagnetic characterization of textured surfaces formed by metallic pins," *IEEE Trans. Antennas Propag.*, vol. 56, no. 2, pp. 405–415, Feb. 2008.
[22] A. Polemi, S. Maci, and P.-S. Kildal, "Dispersion characteristics of a metamaterial-based parallel-plate ridge gap waveguide realized by bed of nails," *IEEE Trans. Antennas Propag.*, vol. 59, no. 3, pp. 904–913, Mar. 2011.
[23] P.-S. Kildal, E. Alfonso, A. Valero-Nogueira, and E. Rajo-Iglesias, "Local metamaterial-based waveguides in gaps between parallel metal plates," *IEEE Antennas Wireless Propag. Lett.*, vol. 8, no. 4, pp. 84–87, Apr. 2009.
[24] P.-S. Kildal, A. U. Zaman, E. Rajo-Iglesias, E. Alfonso, and A. Valero-Nogueira, "Design and experimental verification of ridge gap waveguide in bed of nails for parallel-plate mode suppression," *IET Microw., Antennas Propag.*, vol. 5, no. 3, pp. 262–270, Mar. 2011.
[25] D. Sievenpiper, L. Zhang, R. F. J. Broas, N. G. Alexopolous, and E. Yablonovitch, "High-impedance electromagnetic surfaces with a forbidden frequency band," *IEEE Trans. Microw. Theory Tech.*, vol. 47, no. 11, pp. 2059–2074, Nov. 1999.

[26] R Mittra and S. W. Lee, *Analytical Techniques in the Theory of Guided Waves*. New York, NY, USA: Macmillan, 1971.
[27] V. G. Daniele and R. Zich, *The Wiener-Hopf Method in Electromagnetics*. Rijeka, Croatia: SciTech, 2014.

Enrica Martini (S'98–M'02–SM'13) was born in Spilimbergo, Italy, in 1973. She received the Laurea degree (*cum laude*) in telecommunication engineering and the Ph.D. degree in informatics and telecommunications from the University of Florence, Florence, Italy, in 1998 and 2002, respectively, and the Ph.D. degree in electronics from the University of Nice Sophia Antipolis, Nice, France, in 2002, under joint supervision.

She was with the University of Florence, under a one-year research grant from Alenia Aerospazio Company, Rome, Italy, until 1999. In 2002, she joined the University of Siena, Siena, Italy, as a Research Associate. She was with the Electromagnetic Systems Section of the Ørsted•DTU Department, Technical University of Denmark, Lyngby, Denmark, until 2007. From 2007 to 2017, she was a Post-Doctoral Fellow with the University of Siena. She is currently the Co-Founder and a CEO of the startup Wave Up Srl, Siena. Her current research interests include metamaterial characterization, metasurfaces, electromagnetic scattering, antenna measurements, finite-element methods, and tropospheric propagation.

Dr. Martini was a co-recipient of the 2016 Schelkunoff Transactions Prize Paper Award, the Best Paper Award in Antenna Design and Applications at the 11th European Conference on Antennas and Propagation, and the Hans Christian Ørsted Postdoctoral Fellowship from the Technical University of Denmark in 2005.

Mário G. Silveirinha (S'99–M'03–SM'13–F'14) received the Licenciado degree in electrical engineering from the University of Coimbra, Coimbra, Portugal, in 1998, and the Ph.D. degree in electrical and computer engineering (with a minor in applied mathematics) from the Instituto Superior Técnico (IST), Technical University of Lisbon, Lisbon, Portugal, in 2003.

He is currently a Professor with IST, University of Lisbon, Lisbon, and a Senior Researcher with the Instituto de Telecomunicações, Lisbon. His current research interests include electromagnetism, plasmonics and metamaterials, quantum optics, and topological effects.

Dr. Silveirinha is a Junior Member of the Academy of Sciences of Lisbon. He was a recipient of the 2018 IET Harvey Engineering Research Prize for contributions to electrodynamics of metamaterials and its applications to microwave components and devices.

Stefano Maci (F'04) received the Laurea degree (*cum laude*) from the University of Florence, Florence, Italy, in 1987.

In 2004, he was the Founder of the European School of Antennas, Brussels, Belgium. From 2008 to 2015, he was the Director of the Ph.D. Program in information engineering and mathematics, University of Siena, Siena, Italy, where he has been a Professor since 1997. Since 2010, he has been a Principal Investigator of six cooperative projects financed with the European Space Agency, Noordwijk, The Netherlands. He has authored or co-authored over 150 papers published in international journals, among which 100 are in the IEEE journals, 10 book chapters, and about 400 papers in international proceedings, which have been cited by more than 5700 times. His current research interests include high-frequency and beam representation methods, computational electromagnetics, large phased arrays, planar antennas, reflector antennas and feeds, metamaterials, and metasurfaces.

Prof. Maci was an AdCom Member of the IEEE Antennas and Propagation Society (AP-S), Board of Directors of the European Association on Antennas and Propagation (EurAAP), Antennas and Propagation Executive Board of the Institution of Engineering and Technology, U.K., and the National Italian Committee for Qualification to Professor from 2013 to 2015. He has been a member of the Technical Advisory Board of 11 international conferences and the Review Board of six International Journals, since 2000. He was the Chair of the Award Committee of IEEE AP-S and the Co-Founder of two spin-off companies. He is the Director of the consortium FORESEEN, presently involving 48 European institutions, and a Principal Investigator of the Future Emerging Technology Project Nanoarchitectronics of the eighth EU Framework Program. He was a recipient of the EurAAP Award in 2014, the IEEE Shelkunoff Transaction Prize in 2015, and the Chen-To Tai Distinguished Educator Award in 2016. He is a Distinguished Lecturer of the IEEE AP-S. He has organized 25 special sessions in international conferences and held 10 short courses in the IEEE AP-S Symposia about metamaterials, antennas, and computational electromagnetics. From 2004 to 2007, he was a WP Leader of the Antenna Center of Excellence (FP6-EU). From 2007 to 2010, he was the International Coordinator of a 24-institution consortium of a Marie Curie Action (FP6). He was an Associate Editor of the IEEE TRANSACTIONS ON ANTENNAS AND PROPAGATION.